PERGAMON

Journal of Atmospheric and Solar-Terrestrial Physics 62 (2000) 553–565

Journal of ATMOSPHERIC AND SOLAR-TERRESTRIAL PHYSICS

Determining parameters of large-scale traveling ionospheric disturbances of auroral origin using GPS-arrays

E.L. Afraimovich*, E.A. Kosogorov, L.A. Leonovich, K.S. Palamartchouk, N.P. Perevalova, O.M. Pirog

Institute of Solar-Terrestrial Physics, Siberian Division of the Russian Academy of Sciences (ISTP SD RAS), P.O. Box 4026, Irkutsk, 664033, Russian Federation

Received 18 June 1999; received in revised form 29 November 1999; accepted 5 December 1999

Abstract

The intention in this paper is to investigate the form and dynamics of large-scale traveling ionospheric disturbances (LS TIDs) of auroral origin. We have devised a technique for determining LS TID parameters using GPS-arrays whose elements can be selected from a large set of GPS stations forming part of the International GPS Service network. The method was used to determine LS TID parameters during a strong magnetic storm of September 25, 1998. The North-American sector where many GPS stations are available, and also the time interval 00:00–06:00 UT characterized by a maximum value of the derivative Dst were used in the analysis. The study revealed that this period of time was concurrent with the formation of the main ionospheric trough with a conspicuous southward wall in the range of geographic latitudes 50–60° and the front width of no less than 7500 km. The auroral disturbance-induced large-scale solitary wave with a duration of about 1 h and the front width of at least 3700 km propagated in the equatorward direction to a distance of no less than 2000–3000 km with the mean velocity of about 300 m/s. The wave front behaved as if it 'curled' to the west in longitude where the local time was around afternoon. Going toward the local nighttime, the propagation direction progressively approximated an equatorward direction.

1. Introduction

Many publications, among them a number of thorough reviews (Hunsucker, 1982; Hocke and Schlegel, 1996) have been devoted to the study of large-scale traveling ionospheric disturbances (LS TIDs) with typical periods of 1–2 h and 1000–2000 km wavelengths. It is generally accepted that LS TIDs represent the manifestation of acoustic-gravity waves (AGW) whose generating regions lie in the auroral zones of the northern or southern hemisphere. Therefore, research on LS TIDs can provide important information about the processes occurring in these zones under quiet and disturbed conditions.

However, the basic properties and parameters of LS TIDs are as yet imperfectly understood. Are they a periodic process or a solitary wave (Savina and Erukhimov, 1981; Hunsucker, 1982) propagating to large distances from the source of generation? What is the form and the width of the wave front of LS TIDs?

Measurements of the velocity modulus have been inadequate so far. Some investigators reported markedly differing propagation velocities of LS TIDs — by as many as several thousand meters per second, or in

* Corresponding author. Fax: +7-3952-462-557.
E-mail address: afra@iszf.irk.ru (E.L. Afraimovich).

1364-6826/00/$ - see front matter
PII: S1364-6826(00)00011-0

excess of sound velocities at heights of AGW propagation in the atmosphere (see reviews by Hunsucker, 1982; Hocke and Schlegel, 1996). The amount of published data on LS TID propagation directions is substantially smaller. It is generally believed that they move toward the equator. At the same time some authors reported the detection of a deviation of the azimuth of LS TID propagation from the equatorward direction (Maeda and Handa, 1980; Sharadze et al., 1986; Oliver et al., 1997; Ma et al., 1998; Hall et al., 1999).

Solving the above-mentioned outstanding questions requires appropriate spatial-temporal resolution which cannot be provided by existing highly sparse ionosonde networks, much less by incoherent scatter radars and MST-radars.

An opening shot in a new chapter of remote probing of the ionosphere is the development of a global navigation system GPS and the creation (on its basis) of a far-flung worldwide geodynamic network IGS (International GPS Service) numbering about 220 GPS receivers as of November 1999, and other GPS networks that provide data to public access.

Techniques for determining ionosphere-induced relative variations in total electron content (TEC) from measurements of phase path increments of the GPS transionospheric radio signal were described in detail in an extensive series of publications (Hofmann-Wellenhof et al., 1992; Calais and Minster, 1995, 1996; Fitzgerald, 1997). For this kind of measurements, the error of TEC determination for 30 s intervals of averaging does not exceed 10^{14} m^{-2}, although the initial TEC value remains unknown (Hofmann-Wellenhof et al., 1992). This permits ionization irregularities and wave processes in the ionosphere to be monitored over a wide range of amplitudes (up to 10^{-4} of the diurnal variation of TEC) and periods (from a few hours down to 5 min).

Recently a number of authors (Wilson et al., 1995; Mannucci et al., 1998; Schaer et al., 1998; and others) have developed a new technology for constructing global maps of absolute 'vertical' values of TEC using data from the IGS network (Global Ionospheric Maps — GIM technology). Coupled with the posibility of obtaining these maps in the standard IONEX format (Schaer et al., 1998) on the Internet, the GIM technology provided researchers with a new powerful tool for studying large-scale ionospheric processes under quiet and disturbed conditions on a global scale. This technology has now been used to obtain such new evidence of the global development of large-scale ionospheric disturbances during strong ionospheric storms, which was previously unfeasible with relatively sparse conventional facilities such as ionosondes or even incoherent scatter radars (Ho et al., 1996, 1998; Jakowski et al., 1999).

Ho et al. (1996, 1998) devised a specialized procedure for normalizing TEC maps to background conditions, enabling identification of the 'disturbed' part of a global-time TEC distribution. Using this procedure and 15 min time resolution IONEX maps, Ho et al. (1998) seem to have been the first to discover that LS TIDs that were produced in the auroral zone during the November 26, 1994 magnetic storm propagated equatorward with the mean velocity of 460 m/s and a constant angular moment. However, these results were obtained through a tedious visual examination of TEC maps because quantitative analysis of the TEC dynamics would be impracticable when the data in the IONEX format as such are used.

Spatial interpolation used in constructing maps is a serious problem with the GIM technology. The nonuniform distribution of GPS receivers on the globe, combined with the need to obtain TEC values on a uniform grid for constructing global maps, results in a different data quality in different regions. TEC values represented on maps are accurate for regions with a large number of GPS receivers, but they are less trustworthy where the number of these receivers is small.

Another important limitation of the GIM technology is low resolution of the maps. The authors of this technology (Wilson et al., 1995; Mannucci et al., 1998; Schaer et al., 1998; Ho et al., 1996, 1998) have TEC maps with time steps of 15 min at their disposal. Two hour resolution data are available on the Internet. At the same time, TEC measurements at each particular point of the IGS systems are made with 30 s intervals.

We suggest an alternative method of using the IGS network to determine LS TID characteristics. The method is based on calculating spatial and temporal gradients of electron density from TEC measurements at three spaced IGS stations (GPS-array). It was implemented for determining LS TID parameters during a strong magnetic storm of September 25, 1998. The validity of the method was tested by a computer simulation. A brief account of the proposed method is given in Section 2. Section 3 gives a description of the geomagnetic situation on September 25, 1998, and the experimental geometry. Data from different GPS-arrays are presented in Section 4. Results are discussed and compared with those reported by other authors in Section 5.

2. Methods of determining the form and dynamics of TIDs from TEC measurements acquired by GPS-arrays

The method of determining the form and propagation velocity and direction of TIDs which we suggest in this paper is based on Mercier's (1986) statistical method of analyzing the spatial properties of TEC perturbations, recorded by a radio astronomical interfe-

rometer with a short baseline ('short' in relation to the TID wavelength). In this method, input data represent time dependencies of the TEC spatial derivatives $I'_y(t)$ and $I'_x(t)$ along the directions x (eastward) and y (northward). Essentially, the method implies determining a series of instantaneous values of the azimuth $\alpha(t)$:

$$\alpha(t) = \arctan\left(I'_y(t)/I'_x(t)\right) \tag{1}$$

and thereafter constructing the distribution function of the azimuth $P(\alpha)$ on the selected time interval. The central value of α is used as an estimate of the azimuth of predominant propagation of TIDs (modulo 180°).

Another method reported by Mercier (1986) is based on determining the 'contrast' C, a parameter characterizing the degree of anisotropy of TEC distribution in the antenna array plane. In this case the ratio $C_{x,y}$ is calculated:

$$C_{x,y} = \sigma_X/\sigma_Y, \quad \text{if } \sigma_X > \sigma_Y$$

$$C_{x,y} = \sigma_Y/\sigma_X, \quad \text{if } \sigma_Y > \sigma_X \tag{2}$$

where σ_X and σ_Y are r.m.s. of the series $X(t)$ and $Y(t)$, respectively. $X(t)$ and $Y(t)$ have obtained from the input spatial derivatives $I'_x(t)$ and $I'_y(t)$ by rotating the original coordinate system (x, y) by an angle β:

$$X(t) = I'_x(t)\sin\beta + I'_y(t)\cos\beta$$

$$Y(t) = -I'_x(t)\cos\beta + I'_y(t)\cos\beta \tag{3}$$

Mercier (1986) showed that there exists such an angle of rotation β_0, at which the ratio $C_{x,y}$ becomes maximal and equal to the value of the contrast C. The angle β_0 in this case indicates the direction of TID stretching, and the angle $\alpha_c = \beta_0 + \pi/2$ shows the direction of the wave vector $\boldsymbol{K}$, coincident (with an accuracy of up to 180°) with the propagation direction of TIDs.

Thus Mercier's (1986) method gives no way of calculating the velocity modulus, and all that can be achieved is to determine the degree of anisotropy C and the direction α_c of a normal to the traveling leading edge of TEC. In this case the angle α_c is determined only to within 180°, i.e. the directions α_c and $\alpha_c \pm 180°$ are indistinguishable if the Mercier's method is used.

The above-mentioned estimates will be used later in the text when analyzing the properties of LS TIDs of auroral origin.

In an attempt to achieve a more accurate determination of TID parameters by exploiting the new possibilities made available by the IGS network, Afraimovich et al. (1998) have developed the Statistical Angle-of-Arrival and Doppler Method (SADM–GPS). The method, in essence, implies that not only the spatial $I'_x(t)$, $I'_y(t)$ (as in Mercier, 1986) but also time $I'_t(t)$ derivatives of TEC can be determined from measurements of the total electron content $I(t)$ at three spaced GPS stations (GPS-array). This furnishes a means of uniquely inferring the orientations $\alpha(t)$ of the TID wave vector $\boldsymbol{K}$ in the range 0–360°, as well as determining the velocity modulus $v(t)$.

In a first approximation LS TIDs, which propagate in the equatorward direction from the auroral zone, may be represented as a plane solitary traveling wave (Hunsucker, 1982):

$$I(t, x, y) = \delta(t)\sin\left(\Omega t - K_x x - K_y y + \varphi_0\right) \tag{4}$$

where $I(t, x, y)$ are space-time variations of TEC; $\delta(t) = \exp[-((t - t_{\max})/(t_d))^2]$ are the amplitude; K_x, K_y, Ω are the x- and y-projections of the wave vector $\boldsymbol{K}$, and the angular disturbance frequency, respectively; φ_0 is the initial disturbance phase; $t_{\max}$ is the time when the disturbance has a maximum amplitude, and t_d is the half-thickness of the 'wave packet'.

Using the SADM–GPS algorithm it is possible to determine at every instant the propagation velocity modulus $v(t)$ and the azimuth $\alpha(t)$ of the LS TID motions by formulas:

$$\alpha(t) = \operatorname{atan}\left(u_y(t)/u_x(t)\right)$$

$$u_x(t) = I'_t(t)/I'_x(t) = u(t)/\cos\alpha(t)$$

$$u_y(t) = I'_t(t)/I'_y(t) = u(t)/\sin\alpha(t)$$

$$u(t) = |u_x(t)u_y(t)|/\left(u_x^2(t) + u_y^2(t)\right)^{-1/2}$$

$$v_x(t) = u(t)\sin\alpha(t) + w_x(t)$$

$$v_y(t) = u(t)\cos\alpha(t) + w_y(t)$$

$$v(t) = \left(v_x^2(t) + v_y^2(t)^{1/2}\right) \tag{5}$$

where u_x and u_y are the propagation velocities of the phase front along the axes x and y in a frame of reference related to the GPS-array; w_x and w_y are the x and y projections of the velocity w of the subionospheric point (for taking into account the motion of the satellite).

Let us take a brief look at the sequence of data handling procedures. Out of a large number of IGS stations, three points (A, B, C) are chosen in such a way that the distances between them do not exceed

about one-half the expected wavelength of the disturbance. The point B (a point with the least latitude) is taken to be the center of a topocentric frame of reference whose axes x and y are directed eastward and northward, respectively. Such a configuration of the GPS receivers represents a GPS-array (or a GPS-interferometer) with a minimum of the necessary number of elements. In regions with a dense network of GPS-points, we can obtain a broad range of GPS-arrays of a different configuration, which furnishing a means of testing the data obtained for reliability; in this paper we have taken advantage of this possibility.

Input data for the SADM–GPS are represented by the TEC series $I_A(t)$, $I_B(t)$, and $I_C(t)$, as well as by the corresponding series of values of the angle of elevation $\theta_s(t)$ and the azimuth $\alpha_s(t)$ of the beam to the satellite calculated using our developed program CONVTEC which transforms standard (for the IGS) RINEX-files received from the Internet (Gurtner, 1993).

The series $I_A(t)$, $I_B(t)$, and $I_C(t)$ are calculated from increment data on the phase path of the GPS transionospheric signal at two GPS frequencies L_1 and L_2 contained in the RINEX-file. The method of reconstructing TEC variations from measurements of phase path increments is described in detail and validated in a whole series of publications (for example, Hofmann-Wellenhof et al., 1992).

It is significant that the most reliable results derived from determining the TID structure and dynamics correspond to high values of the angle of elevation $\theta(t)$ of the beam to the satellite because the effects of sphericity and nonuniformity of the TEC perturbation become sufficiently small in this case.

Furthermore, in consequence of the dependence of the TEC variation amplitude on the angle between the TID propagation direction and the beam direction to the satellite, the TEC variation amplitude for some of the satellites monitored by a given interferometer can be below the noise level of measurements (this effect is considered in greater detail by Afraimovich et al. (1998)). These two considerations dictated our selection of the satellite to receive the initial data at each GPS-array. We simply disregarded the satellites with elevations below 30°, while for obtaining the series $I_A(t)$, $I_B(t)$, and $I_C(t)$ at each interferometer, the satellite was selected, which was closest to the zenith and provided a maximum response in TEC variations.

Note also that when calculating LS TID parameters by the SADM–GPS method, no reduction of the series $I_A(t)$, $I_B(t)$, and $I_C(t)$ to a vertical TEC is needed, and we did not do this.

For determining LS TID propagation characteristics, use is made of continuous series of measurements of $I_A(t)$, $I_B(t)$, and $I_C(t)$ of a length of two-three hours at least. Variations of the regular ionosphere, and also trends introduced by the motion of the satellite are eliminated using the procedure of filtering the TEC perturbation by removing the trend with third-to-fifth order polynomials.

Linear transformations of the differences of the values of the filtered TEC $(I_B - I_A)$ and $(I_B - I_C)$ at the receiving points A, B and C are used to calculate the components of the TEC gradient I'_x and I'_y (Afraimovich et al., 1998). The time derivative of TEC I'_t is determined by differentiating $I_B(t)$ at the point B.

The resulting series $I'_x(t)$, $I'_y(t)$ and $I'_t(t)$ are used to calculate instantaneous values of the velocity modulus $v(t)$ and the azimuth $\alpha(t)$ of TID propagation. Concurrent with this procedure, a correction for the motion of the satellite is introduced into calculations using current information about the satellite's angular coordinates (formulas (5)).

Next, the series $v(t)$ and $\alpha(t)$ are put to a statistical treatment. This involves constructing distributions of the velocity $P(v)$ and direction $P(\alpha)$ which are analyzed to test the hypothesis of the existence of the preferred propagation direction. If such a direction does exist, then the corresponding distributions are used to calculate the mean value $\langle v \rangle$ and the r.m.s. σv of the velocity modulus, as well as the mean value $\langle \alpha \rangle$ and the r.m.s. $\sigma\alpha$ of the azimuth of TID propagation.

Thus, through the use of the transformations (5) we obtain the following parameters characterizing the TID dynamics: T_0 is the start of measurements; dT is the time interval of measurements; A is the amplitude of the filtered TEC which is determined as the r.m.s. of the series $I_B(t)$; $\langle \alpha \rangle$ and $\sigma\alpha$, respectively, are the mean value and the r.m.s. of the LS TID propagation direction; and $\langle v \rangle$ and σv, respectively, are the mean value and the r.m.s. of the velocity modulus.

We have also performed calculations of the quantities characterizing the form of LS TIDs, namely the contrast C and the angle α_c by the method of Mercier (1986), i. e. using formulas (1) and (2).

Also for comparison purposes, we resorted to a possibility of estimating the LS TID propagation velocity from the time lag of such TEC variations at meridionally spaced points. For the central point of each array, we decided to choose a longitudinally near-lying but higher-latitude calibrating station, at which TEC variations had the character similar to those at the central point but occurring somewhat earlier. This time lag was used to determine the LS TID propagation velocity v_r along the calibrating station — GPS-array central point line.

In summarizing the description of our proposed SADM–GPS method, it can be said that it opens up new avenues for the study of traveling ionospheric disturbances. The combined use both of the spatial TEC derivatives and of the time TEC derivative (formulas (5)), unlike the Mercier method, makes it possible to uniquely determine the orientation $\alpha(t)$ of the TID

wave vector $\boldsymbol{K}$ in the range 0–360°. Furthermore, it becomes possible to calculate the velocity modulus $v(t)$, which the Mercier technique simply does not consider. Multi-satellite radio interferometry using the SADM–GPS algorithm enables detection and measurement of the TID velocity vector over almost the entire range of possible propagation directions of TIDs (Afraimovich et al., 1998). Unlike the GIM technology, the SADM–GPS method is a relatively simple and convenient tool for quantitative analysis of the TEC dynamics. The implementation our method at the far-flung IGS network would provide a global picture of the LS TID velocity field thus making it possible to solve a number of important questions of characteristics of these ionospheric disturbances.

3. Characteristics of the geomagnetic situation on September 25 1998, and the experimental geometry

Our developed method was implemented for determining LS TID parameters during a strong geomagnetic disturbance on September 25, 1998. On that day, Dst-variations showed a large storm with a maximum amplitude of 233 nT. Kp in the storm maximum were as high as 8, and the sum of Kp for 24 h was 48 on September 25. Unfortunately, this storm developed at a sufficiently disturbed background: the day before, September 24, the sum of Kp was 29, with the values of Dst-variations fluctuating about −50 nT. At 01:00 UT on September 25, the Dst-variation increased abruptly to 0; after that, it began to decrease rapidly and dropped to −220 nT at 07:00 UT and to −233 nT at 10:00 UT. This was followed by the recovery phase which persisted until September 30.

Within the context of this study, we will focus our attention on the determination of the LS TID properties which occurred in the auroral zone in the most interesting time interval 00:00-04:00 UT characterized by the largest value of the Dst-derivative. The values of Dst-variation and Kp-index for September 24 and 25 are shown in Fig. 1, panels c and d. Panels a and b in Fig. 1 present TEC variations at a set of auroral stations in the North-American sector for the same period, 24–25 September 1998. The North-American sector was used in the analysis primarily because many GPS-stations of the IGS network are located in this region. It is also significant that at the beginning of the above-mentioned time interval and in the selected longitude range the local time varied from 14 to 19 LT, which gives grounds to interpret the results obtained as being characteristic for the daytime and evening hours.

The map of the experiment on September 25, 1998 in the geographic coordinate system in the range 30–70°N and 200–300°E is presented in Fig. 2. Cross indicates the position of the north magnetic pole (NMP). Values of local time LT corresponding to the universal time 00:00–04:00 UT are shown at a given longitude range.

Of the large number of IGS stations in the North-American sector, we chose a set of auroral stations, the data from which illustrate the ionospheric TEC variations behavior during the beginning of geomagnetic disturbance of September 25, 1998.

The location of these auroral sites is designated on the Fig. 2 map by heavy dots. Also shown are the names of those auroral stations which were subsequently used as calibrating sites in a comparative evaluation of the TID velocity (see Section 4). Geo-

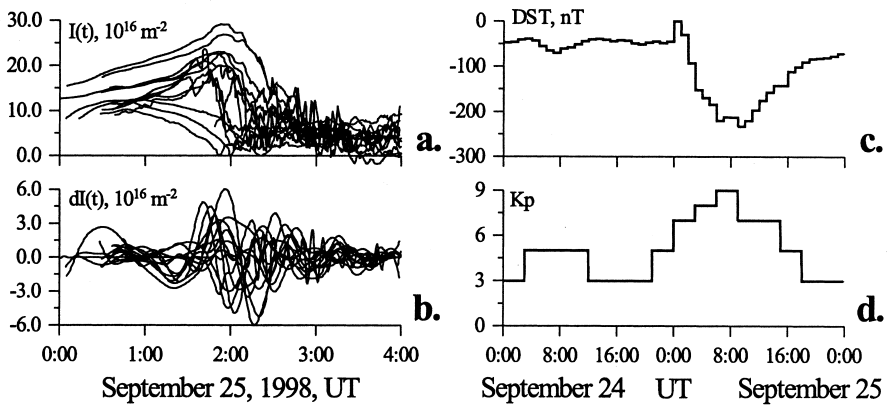

Fig. 1. Dst-variations of the geomagnetic field — panel c and Kp-index — panel d during a strong geomagnetic storm of September 24–25, 1998. Maximum values of the derivative of Dst variations were observed from 00:00 to 04:00 UT on September 25, 1998. Initial TEC series $I(t)$ — panel a and filtered (with the trend removed) series $dI(t)$ — panel b as obtained during this time interval for the set of auroral stations shown by heavy dots in Fig. 2.

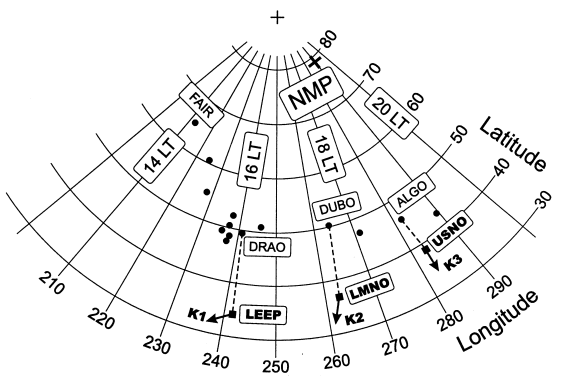

Fig. 2. Map of the September 25, 1998 experiment in the geographic coordinate system in the range 30–70° N and 200–300° E. Heavy dots show those sites of the IGS network, the set of auroral stations, for which an abrupt decrease of TEC was observed during 01:30–02:30 UT; names of several sites are also given here. These dots give an idea of the location of the southward wall of the main ionospheric trough. The position of the north magnetic pole (NMP) is shown by a cross. Black boxes and site names next to them represent the location of central sites of GPS-arrays. Calibrating GPS-stations and central sites of GPS-arrays are connected by dashed lines. The arrows represent the direction of the wave vector $\boldsymbol{K}$ of LS TIDs as determined by the SADM–GPS method for the GPS-arrays selected. Values of local time LT corresponding to the universal time 00:00 UT are shown for a given longitude range.

graphic and geomagnetic coordinates of the auroral stations are listed in Table 1. Calibrating sites are shown in bold.

The initial TEC series $I(t)$ for the same satellite, PRN19, for the time interval 00:00–04:00 UT, which were calculated for the stations of this set and were brought to the 'vertical' value by the familiar technique (Calais and Minster, 1995, 1996), and also the filtered series $\mathrm{d}I(t)$ are presented in Fig. 1 on panels a and b, respectively. The initial series were reduced to a vertical TEC for illustrative purposes in order to exclude the dependence of the TEC amplitude on satellite elevation.

Our selection of the same satellite, PRN19, for the entire set of the auroral stations was dictated by the same considerations as used in the analysis of the data for each GPS-array (see Section 2): a maximum TEC response, and the satellite proximity to the zenith. For PRN19, a maximum value of elevation $\theta(t)$ of the beam to the satellite during 01:30–02:30 UT for all stations of the auroral chain exceeded 50°. In addition, this minimized the possible conversion error of the TEC value to a 'vertical' value as a consequence of sphericity.

Almost all of auroral stations exhibit a gradual growth of TEC until about 02:00 UT, as well as an abrupt decrease and a pronounced inhomogeneous structure of TEC subsequent to the intersection of this time mark. The filtered series $\mathrm{d}I(t)$ for almost all sites are characterized by the largest oscillation range in the time interval 01:30–02:30 UT.

One plausible interpretation of these data implies that the beams to the satellite in the given time interval intersected the southward wall of the main ionospheric trough (MIT). Similar results from a chain of ionosondes were reported by Whalen (1987). Fig. 2 can also be used to infer the MIT front width as the difference of the longitudes of the marginal points of the

Table 1
GPS site names and locations

No.	SITE	Geographic latitude	Geographic longitude	Geomagnetic latitude	Geomagnetic longitude
1	AIS1	55.069	228.401	59.060	284.377
2	**ALGO**	45.955	281.929	56.870	350.880
3	**DRAO**	49.322	240.376	56.006	299.832
4	**DUBO**	50.258	264.134	61.015	330.516
5	FAIR	64.978	212.501	65.456	263.533
6	KEW1	47.227	271.376	58.612	341.641
7	NANO	49.294	235.914	55.007	294.842
8	POR2	43.070	289.291	53.730	7.532
9	PRDS	50.871	245.707	58.674	305.602
10	SEAT	47.653	237.691	54.647	297.183
11	SEDR	48.521	237.777	54.647	297.183
12	WHIT	60.750	224.778	63.838	277.601
13	WILL	52.236	237.833	58.351	295.814
14	WSLR	50.126	237.079	56.086	295.805
15	**KELY**	66.987	309.056	73.518	40.982
16	MAC1	−54.499	158.935	−64.733	248.305

auroral stations chain. It is seen that in the present study the MIT front width exceeds 80°, or 7500 km. This is also consistent with the data reported by Whalen (1987) and by Hajkowicz and Hunsucker (1987).

An important point within the framework of this paper is that throughout the set of auroral stations the depth of the MIT inferred from the value of relative variation (abrupt decrease) of TEC reached a very large value (from 15 to 25 TECU, TECU $=10^{16}$ m^{-2}). According to the concepts summarized in a review by Hunsucker (1982), such an extended region of the auroral ionosphere that was disturbed so rapidly from an equilibrium condition for a short time interval, must become a source of strong LS TIDs propagating toward the equator. It is worth noting again that this time interval was characterized by the largest value of the Dst-derivative (Fig. 1c), which is in agreement with a similar inference drawn by Ho et al. (1998).

For a reliable determination of LS TID characteristics, it was necessary to detect them at distances larger than the expected wavelength (over 1000 km) and along the entire expected wave front (up to several thousand kilometers). It is primarily these considerations which dictated the selection of corresponding GPS-arrays. Furthermore, it was important to choose areas with a sufficiently dense network of stations such as to ensure appropriate distances between sites of the GPS-arrays. The greatest scope for study was provided by the area of South California with as many as several tens of IGS sites.

The GPS-arrays of the North American sector are shown in Fig. 2 as black boxes. Next to them, names of central sites of the arrays are given. Central sites of the GPS-arrays and corresponding to them calibrating GPS stations are connected by dashed lines: DRAO-LEEP; DUBO-LMNO; ALGO-USNO. This paper is primarily devoted to the study of LS TID characteristics at these arrays. In addition to assess the presence of TIDs in other geographic regions we succeeded in select a further two suitable arrays: one in England (with central site BRUS), and the other in the southern hemisphere (with central site ORRO, Australia). They are not shown in Fig. 2. Geographic coordinates of all sites used as GPS-array elements are presented in Table 2. Items 1–13 of Table 2 correspond to the North American sector, items 14–16 refer to England, and items 17–19 correspond to the southern hemisphere. Central sites of the arrays in the table are in bold.

Table 2
GPS interferometers names and locations

No.	SITE	Geographic latitude	Geograpic longitude
1	BRAN	34.185	241.723
2	CSDH	33.861	241.743
3	CVHS	34.082	242.098
4	DYHS	33.938	241.874
5	**LEEP**	34.134	241.678
6	UCLP	34.069	241.558
7	UCS1	34.024	241.715
8	**LMNO**	36.685	262.519
9	HVLK	37.651	260.893
10	VCIO	36.071	260.783
11	HNPT	38.588	283.870
12	**USNO**	38.918	282.934
13	VIMS	37.608	284.313
14	**BRUS**	50.797	4.359
15	DOUR	50.094	4.594
16	WARE	50.689	5.245
17	**ORRO**	−35.636	148.939
18	STR1	−35.316	149.010
19	TID1	−35.400	148.980

4. The form and dynamics of LS TIDS as deduced from interferometer data

The data obtained from each GPS-array labeled in Fig. 2 were processed in full conformity with the pro-

Table 3
LS TID parameters as derived from GPS measurements

No.	SITE	PRN	T_0 (UT)	dT (min)	A (TECU)	C	α_c (°)	$\langle\alpha\rangle$ (°)	$\sigma\alpha$ (°)	$\langle v\rangle$ (m/s)	σv (m/s)	v_r (m/s)
1	LEEP, CVHS, DYHS	19	2.28	90	2.634	4.5	75	245	22	254	148	212
2	TEST	19	2.28	90	3.320	120	70	245	1	277	151	
3	USC1, UCLP, LEEP	19	2.30	90	2.498	2.3	95	260	28	362	224	
4	DYHS, BRAN, UCLP	19	2.31	90	2.560	2.6	80	249	27	322	204	
5	CVHS, LEEP, CSDH	19	2.32	90	2.595	3.5	65	236	23	351	218	
6	LMNO, HVLK, VCIO	19	2.82	120	0.480	7.1	20	195	24	264	236	238
7	USNO, HNPT, VIMS	31	2.41	120	0.648	3.0	5	177	37	211	138	154
8	BRUS, DOUR, WARE	21	3.58	60	0.335	8.9	180	175	17	286	244	364
9	ORRO, TID1, STR1	06	7.72	60	0.958	1.3	150	331	44	324	158	241

cedures and formulas described in Section 2. The corresponding parameters set out at the end of Section 2 are collected in Table 3. In Fig. 2, the arrows issuing out of the corresponding box labeling the central site of the GPS-array represent schematically the direction of wave vectors $\boldsymbol{K}$ characterized by the respective values of the direction $\langle\alpha\rangle$ LS TIDs. The vectors $\boldsymbol{K}_1, \boldsymbol{K}_2$ and $\boldsymbol{K}_3$ refer to the data from the LEEP (the interferometer LEEP, CVHS, DYHS — line 1 in Table 3), LMNO (line 6 in Table 3) and USNO (line 7 in Table 3) arrays.

Figs. 3 and 4 present the time dependencies of the initial $I(t)$ (panels a and e) and filtered $dI(t)$ (panels b and f) TEC series for the central site of each GPS-array. Names of the central sites and GPS satellite numbers, for which the data were obtained, are given in bold print. The selection of the satellite is explained in Section 2. For comparison, the panels present also the plots of $I(t)$ and $dI(t)$ for calibrating sites from the set of auroral stations whose names are given in small print.

For qualitative comparison with the data from the North-American sector, Fig. 5 presents results for the GPS-arrays located in England and in the eastern part of the southern hemisphere.

The outliers of the direction and velocity in Figs. 3–5, panels c, d, g, and h, are due to a simplified approach to modeling TIDs when developing SADM–GPS. SADM–GPS assumes that a TID has an ideal plane front described by formula (4), which is equivalent to the neglect of second-order correction when deriving formulas (5). In real situations, however, fronts can be more complicated in shape where nonsimulta-

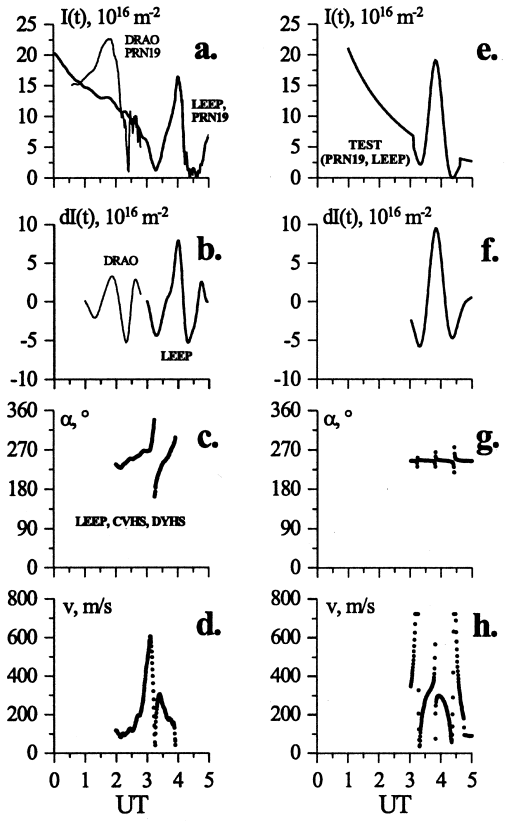

Fig. 3. Time dependencies of the input $I(t)$ — panels a, e and filtered $dI(t)$ TEC series — panels b, f; the direction of the wave vector $\alpha(t)$ — panels c, g and the phase velocity modulus $v(t)$ of LS TIDs — panels d, h as determined for the LEEP array by the SADM–GPS method. Name of central site of GPS-array and PRN numbers are given on panels a, e. Thin lines in panels a, b, e, f show the dependencies $I(t)$ and $dI(t)$ for the calibrating site whose name is given in light print. Panels e–h show calculated data for the TID model in the form of a solitary traveling wave with 90-min period, with 130-min duration of the packet, the maximum amplitude of 0.5 TECU, the horizontal velocity $v = 157$ m/s, and with the azimuth $\alpha = 240°$, as it can be observed by LEEP array at the viewparh to PRN19 satellite.

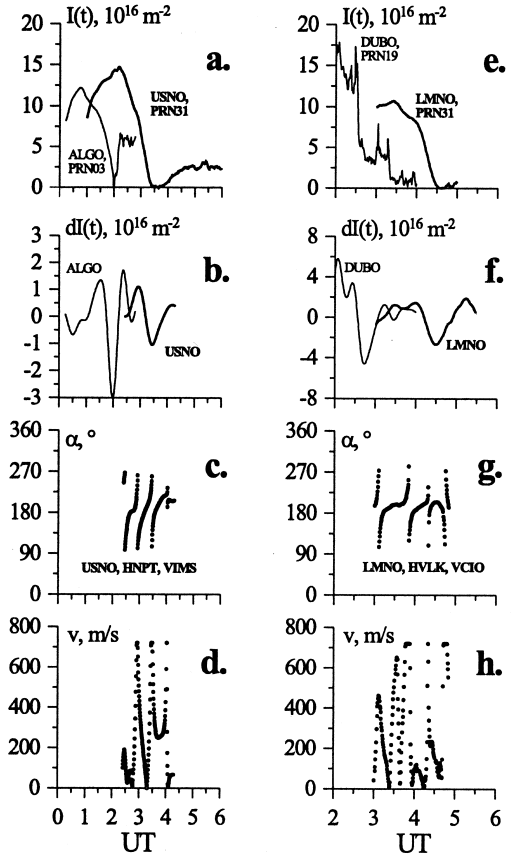

Fig. 4. Same as experimental data for the LEEP array, but for the USNO array (left) and the LMNO array (right).

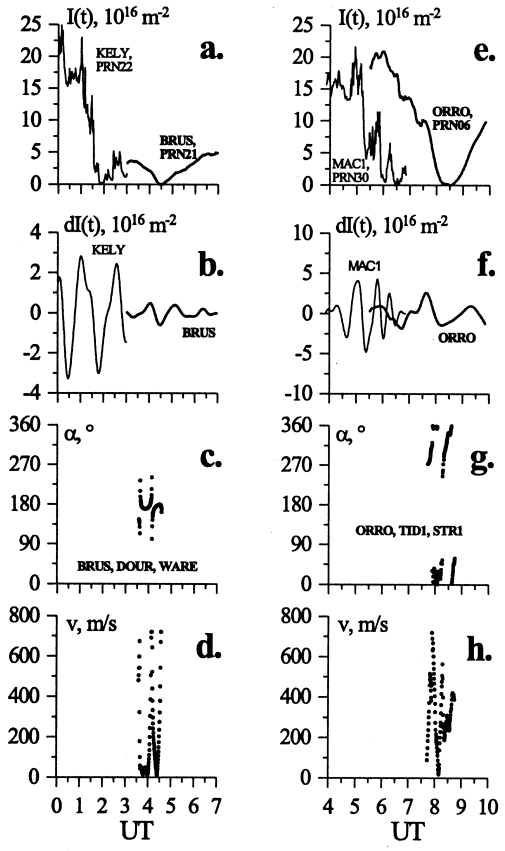

Fig. 5. Same as experimental data for the LEEP array, but for the BRUS array (left) and the ORRO array (right).

neous changes of signs of $I'_x(t)$, $I'_y(t)$, and $I'_t(t)$, which are impossible in the case of a perfectly plane front, can give 'whistlers' as observed in Figs. 3–5. However, a verification of SADM–GPS, described by Afraimovich et al. (1998), revealed that with a statistical approach to the resulting series of TID directions and velocities, their mean values inferred using SADM–GPS are similar to true ones. Thus the outliers are an artifact; they are actually nonexistent and do not interfere with a further statistical analysis of the data.

4.1. Data from the LEEP GPS-array

This interferometer consists of three stations: LEEP, CVHS, and DYHS. The distances between the central and outlying sites do not exceed 40 km. It is clearly seen in Fig. 3a that a sharp TEC peak $I(t)$ occurred at 03:10 UT (19:10 LT) at the LEEP station at the background of a quiet evening decrease in TEC, which is quite extrinsic to this time of day for magnetically quiet conditions but is highly characteristic for TEC variations as pointed out by many authors for similar disturbed conditions (for example, Yeh et al., 1994).

The filtered series $dI(t)$ on panel b during 03:10–05:00 bring out the presence of strong TEC oscillations of the solitary wave type with a period of about one hour and the amplitude $A = 2.6$ TECU. Not only does the range of the filtered $dI(t)$ oscillations exceed the error of phase measurements (10^{-2} m^{-2} TECU), but it also is one order of magnitude larger than the greatest level of TEC variations in the range of TID periods characteristic for quiet conditions (Hunsucker, 1982; Afraimovich et al., 1999).

Such TEC variations (Fig. 3a and b) were observed approximately two hours earlier at the DRAO station located at the distance of 1659 km along the great-circle arc to the north of the LEEP array (see Fig. 2). This delay corresponds to the velocity v_r of LS TID propagation along the DRAO-LEEP line, equal to 212 m/s (line 1 in Table 3).

Fig. 3 presents the time dependencies of the direction $\alpha(t)$ — panel c and the phase velocity modulus $v(t)$ of LS TIDS — panel d as determined for the LEEP array using the SADM–GPS method by formulas (5). Corresponding values of statistical characteristics set out at the end of Section 2 are given in line 1 of Table 3.

The mean value of the velocity modulus $\langle v \rangle$ is 254 m/s, which, with the period of the wave of about 1 h, corresponds to 1000 km wavelength, typical of LS TIDs (Hunsucker, 1982). It is close to the value of $v_r = 212$ m/s as determined from the wave delay along the DRAO-LEEP line.

Comparative calculations by the Mercier method showed primarily a large value of contrast $C = 4.5$ characterizing a high degree of anisotropy of the traveling solitary wave. The azimuth from the contrast was 75° (line 1 of Table 3). Considering that in the Mercier technique α_c is determined only to within 180° (see Section 2), it may be assumed that $\alpha_c = \alpha_c + 180° = 255°$. It is evident that α_c is close to the mean value of $\langle \alpha \rangle = 245°$ calculated by the SADM–GPS method. Thus the two methods give similar values of the LS TID propagation direction, and this direction differs noticeably from the equatorward direction.

4.2. Testing LS TID parameter measurements for reliability

As an assurance of the reliable determination of the main parameters of the form and dynamics of LS TIDs by formulas (5), in the area of South California near the LEEP array we chose other variants of GPS-arrays and processed the data from the PRN19 satellite with the same processing parameters as for the LEEP array. Statistical data presented in Table 3 (lines

3–5) show an agreement of the mean values within their r.m.s, which is testimony to good stability of the acquired data irrespective of the GPS-array configuration.

We availed ourselves also of another method of testing the data from the GPS-array for reliability — by modeling a disturbed TID with specified properties described by Afraimovich et al. (1998), using the algorithm of TEC calculation along the 'receiver-satellite' beam for a typical model of the regular ionosphere. A special feature of this algorithm is that it is possible to calculate TEC for a particular chosen array and for the actual satellite trajectory determined by the broadcast navigation information.

In Fig. 3, panels e–h show calculated data for the LEEP-array and for the TID model in the form of a solitary traveling wave with 90-min period, 130-min duration of the packet, the maximum amplitude of 0.5 TECU, the horizontal velocity $v = 157$ m/s, and the azimuth $\alpha = 240^\circ$. A comparison of these parameters with corresponding values resulting from a processing by formulas (5) (line 2 in Table 3) shows a satisfactory agreement of these values. In Fig. 3, one can also notice a good agreement of experimental (LEEP array) and model variations of TEC $I(t)$, $\mathrm{d}I(t)$ and the dependencies $v(t)$ and $\alpha(t)$.

4.3. Data from other GPS-arrays

For the same time interval as for LEEP, Fig. 4 presents the time dependencies of TEC $I(t)$ — panel e, filtered series $\mathrm{d}I(t)$ — panel f, as well as the directions $\alpha(t)$ — panel g and phase velocity moduli $v(t)$ of LS TIDs — panel h as determined for the LMNO-array. Corresponding values of statistical characteristics are given in line 6 of Table 3. One can notice the proximity of all mean values to corresponding parameters for the LEEP-array, except that the mean value of $\langle\alpha\rangle$ is now closer to the equatorial value (195°) and the wave amplitude is by a factor of 5 smaller than that for LEEP. The mean value of the velocity modulus $\langle v\rangle$, equal to 264 m/s, is also close to the value of $v_r = 238$ m/s determined from the wave delay along the DUBO-LMNO line.

Similarly, Fig. 4 presents the time dependencies of TEC $I(t)$ — panel a, filtered series $\mathrm{d}I(t)$ — panel b, as well as the directions $\alpha(t)$ — panel c, and phase velocity moduli $v(t)$ of LS TIDs — panel d, as determined for the USNO-array. Corresponding values of statistical characteristics are given in line 7 of Table 3. Unlike LEEP and LMNO, the direction of LS TID propagation is nearly equatorward, and the mean value of the velocity modulus $\langle v\rangle$ is markedly smaller (211 km/s). Also, the value of v_r determined from the wave delay along the ALGO-USNO line is still smaller (154 m/s).

For the time interval 00:00–07:00 UT, Fig. 5 presents the time dependencies of TEC $I(t)$ — panel a, filtered series $\mathrm{d}I(t)$ — panel b, as well as the directions $\alpha(t)$ — panel c, and phase velocity moduli $v(t)$ of LS TIDs — panel d, as determined for the BRUS array in England — see also line 8 of Table 3. The mean values are very close to corresponding parameters for the LMNO array. However, $\langle v\rangle$ equal to 286 m/s is markedly smaller than the value of $v_r = 364$ m/s as determined from the wave delay along the KELY-BRUS line.

Some authors pointed out a similarity or even a synchronism of the generation of LS TIDs in the northern and southern hemisphere during geomagnetic disturbances (Hajkowicz and Hunsucker, 1987). Unfortunately, the possibilities of choosing a suitable array in the southern hemisphere have been hitherto limited because of relatively sparse coverage of the IGS network. For the time interval described here, we were able to locate only one GPS-array ORRO, the data from which are presented in Fig. 5 (panels e–h) and in line 9 of Table 3. As expected, the propagation direction $\langle\alpha\rangle$ was equatorward as before; however, a marked (by 30°) westward deviation of the direction must also be pointed out in this case.

5. Discussion and conclusions

Let us now discuss the main results of this study and compare them with findings of other authors.

5.1. Phase velocity of LS TID propagation

As has been pointed out in Section 1, some researchers have reported markedly differing values of the LS TID propagation velocity — by as many as several thousand m/s, or exceeding the sound velocity at heights of AGW propagation in the atmosphere (see reviews of Hunsucker, 1982; Hocke and Schlegel, 1996). In the Table 4, we included some selected data to illustrate the large spread in LS TID velocities.

High velocity values were obtained for the most part at meridionally spaced 'chains' of ionosondes (as far as was allowed by actual possibilities). For example, Hajkowicz and Hunsucker (1987), by investigating the propagation of LS TIDs from variations of F-region effective heights in the northern and southern hemisphere, found that large-scale disturbances of ionization propagate equator-ward with the velocity of about 800 m/s and have a constant period of about 135 min in both hemispheres. Similar results were obtained at spaced sites of TEC measurement from geostationary satellite signals and from ionosonde chains in a paper of Yeh et al. (1994).

The authors of the cited papers constructed a dependence of the time delay of similar disturbances of the received signal parameters on the latitude of the point of observation. Therefore, the meridional velocity component of the disturbance front rather than the true phase velocity of LS TID propagation was actually estimated. This velocity was equal to the phase velocity, provided that LS TIDs propagated exactly equatorward. With a marked deviation from the southward direction, such a method could give obviously too high estimates of the propagation velocity of LS TIDs. For the LEEP array, for example, where we observed the largest possible (in relation to the data from the other arrays) deviation from the equatorward direction of LS TID propagation, such an apparent velocity value would be 604 m/s, or more than twice as large as the true value of the phase velocity (254 m/s).

It is worth noting that whenever the spaced beam reception method was used at the EISCAT incoherent scatter station to determine the velocity and direction of LS TIDs (Ma et al., 1998), the resulting estimates of the phase velocity of LS TID propagation did not exceed 400 m/s. Still smaller values of the phase velocity of LS TIDs (averaging about 240 m/s) were measured at the MU radar (Oliver et al., 1997). Similar estimates of the LS TID velocity (from 50 to 280 m/s) were obtained at Super-DARN (Hall et al., 1999). These data are in good agreement with the mean value of the phase velocity which we have obtained by taking into account the data from all arrays listed in Table 3 (300 m/s).

5.2. The propagation direction and the form of the wave front of LS TIDS

For all arrays, the cross-section of the wave front along the propagation direction was more likely to correspond to a solitary traveling wave than to a periodic process, which is consistent with the data reported by other authors (Savina and Erukhimov, 1981; Hunsucker, 1982). According to our data, the large-scale solitary wave with a duration of about 1 hour that was produced by an auroral disturbance, propagated in the equatorward direction to a distance of at least 2000-3000 km with the mean velocity of about 300 m/s.

The direction of the wave vector $\boldsymbol{K}$ varied along the wave front from 245° in the LEEP array longitude and 195° in the LMNO longitude to 177° in the USNO longitude. On the map in Fig. 2, this is plotted by the vectors $\boldsymbol{K}_1$, $\boldsymbol{K}_2$ and $\boldsymbol{K}_3$, respectively. The wave front behaved as if it 'curled' to the west in longitude where the local time was around afternoon. Going toward the local nighttime, the propagation direction approached the equatorward propagation.

One way of explaining the westward displacement of the propagation direction of LS TIDs could be based on the well-known difference of the positions of the geographic and geomagnetic poles subject to the condition that the region generating LS TIDs in the auroral zone is symmetric about the geomagnetic pole. In our case we can not agree with such an explanation (see in Fig. 2 the relative position of the north geomagnetic pole NMP and of the set of auroral stations designating the boundary of the generating region of LS TIDs).

Published data on propagation directions of LS TIDs are very few in number. It is generally believed that they move toward the equator (see Table 4). We are aware only of a few papers where numerical values of the propagation azimuth of LS TIDs are given and its westward displacement by 10–20° on average is determined, which is consistent with the concept of the Coriolis force effect on the AGW propagation in the atmosphere (Maeda and Handa, 1980; Sharadze et al., 1986; Oliver et al., 1997; Ma et al., 1998; Balthazor and Moffett, 1999; Hall et al., 1999). Our data may be treated as supporting this hypothesis.

Another way to explain such a structure of disturb-

Table 4
LS TID parameters as derived from techniques other than GPS

No.	Reference	Observer	$\langle\alpha\rangle$ (°)	$\sigma\alpha$ (°)	$\langle v\rangle$ (m/s)	σv (m/s)
1	Maeda and Handa (1980)	Ionosonde	197	34	600	
2	Hall et al. (1999)	SuperDARN	187	17	114	43
3	Sharadze et al. (1986)	Ionosonde	South-westward		200–600	
4	Hajkowicz and Hunsucker (1987)	Ionosonde	Equatorward		800	
5	Rice et al. (1988)	IS Radar	Equatorward		454	67
6	Rice et al. (1988)	EISCAT	Equatorward		425	50
7	Natorf et al. (1992)	EISCAT	Equatorward		400	
8	Oliver et al. (1997)	MU	Southward		240	
9	Ma et al. (1998)	EISCAT	Southward		170	
10	Yeh et al. (1994)	Ionosonde, TEC/Geostationary satellite	Equatorward		330–680	
11	Ho et al. (1998)	TEC/GPS	Southward		460	

ance wave front was proposed by Foster et al. (1989). According to his model, 'curling' of the disturbance front is the effect of great stream of plasma, ejected from rotating sun-ward polar cap.

However, more reliable conclusions require expanding considerably the sample statistic of GPS-arrays used in the analysis of LS TIDs of auroral origin.

Our developed technique can be useful for a detailed global-scale investigation of large-scale wave processes generated in the auroral zone during disturbances; during solar eclipses as the Moon's shadow crosses through the terrestrial surface with supersonic speed; at the time of volcanic eruptions, as well as for detecting powerful artificial modifications of the Earth's atmosphere.

Acknowledgements

We are grateful to A.V. Tashchilin, N.N. Klimov, E.A. Ponomarev, and A.D. Kalikhman for their encouraging interest in this study and active participations in discussions. We are also indebted to T.G. Pirog for preparing the input data. We are grateful to IGS for data of excellent quality. Thanks are also due V.G. Mikhalkovsky for his assistance in preparing the English version manuscript. This work was done with support from the Russian Foundation for Basic Research (grants 97-02-96060 and 99-05-64753), as well as RF Minvuz Grant 1999; supervisor B.O. Vugmeister.

References

Afraimovich, E.L., Palamartchouk, K.S., Perevalova, N.P., 1998. GPS radio interferometry of traveling ionospheric disturbances. Journal of Atmospheric and Solar-Terrestrial Physics 60, 1205–1223.

Afraimovich, E.L., Boitman, O.N., Kalikhman, A.D., Pirog, T.G., Zhovty, E.I., 1999. Dynamics and anisotropy of traveling ionospheric disturbances as deduced from transionospheric sounding data. Radio Science 34, 477–487.

Balthazor, R.L., Moffett, R.J., 1999. Morphology of large-scale traveling atmospheric disturbances in the polar thermosphere. Journal of Geophysical Research 104 (A1), 15–24.

Calais, E., Minster, J.B., 1995. GPS detection of ionospheric perturbations following the January, 1994 Northridge earthquake. Geophysical Research Letters 22, 1045–1048.

Calais, E., Minster, J.B., 1996. GPS detection of ionospheric perturbations following a Space Shuttle ascent. Geophysical Research Letters 23, 1897–1900.

Fitzgerald, T.J., 1997. Observations of total electron content perturbations in GPS signals caused by a ground level explosion. Journal of Atmospheric and Terrestrial Physics 59, 829–834.

Foster, J.C., Turunen, T., Pollari, P., Kohl, H., Wickwar, V.B., 1989. Multi-radar mapping of auroral convection. Advances in Space Research 9 (5), (5)19–(5)27.

Gurtner, W., 1993. RINEX: The Receiver Independent Exchange Format Version 2.http://igscb.jpl.nasa.gov:80/igscb/data/format/rinex2.txt.

Hajkowicz, L.A., Hunsucker, R.D., 1987. A simultaneous observation of large-scale periodic TIDs in both hemispheres following an onset of auroral disturbances. Planetary Space Science 35 (6), 785–791.

Hall, G.E., Cecile, J.F., MacDougall, J.W., St.Maurice, J.P., Moorcroft, D.R., 1999. Finding gravity wave source positions using the Super Dual Auroral Radar Network. Journal of Geophysical Research 104 (A1), 67–78.

Ho, C.M., Lindqwister, U.J., Mannucci, A.J., Pi, X., Tsurutani, B.T., 1996. Global ionosphere perturbations monitored by the worldwide GPS network. Geophysical Research Letters 23, 3219–3222.

Ho, C.M., Iijima, B.A., Lindqwister, X.P., Mannucci, A.J., Sparks, L., Reyes, M.J., Wilson, B.D., 1998. Ionospheric total electron content perturbations monitored by the GPS global network during two northern hemisphere winter storms. Journal of Geophysical Research 103, 26409–26420.

Hofmann-Wellenhof, B., Lichtenegger, H., Collins, J., 1992. Global Positioning System: Theory and Practice. Springer-Verlag, Wien, New York.

Hocke, K., Schlegel, K., 1996. A review of atmospheric gravity waves and traveling ionospheric disturbances: 1982–1995. Annales Geophysic 14, 917–940.

Hunsucker, R.D., 1982. Atmospheric gravity waves generated in the high-latitude ionosphere: a review. Review of Geophysics 20, 293–315.

Jakowski, N., Sardon, E., Schluter, S., 1999. Total electron content of the ionosphere during the geomagnetic storm on 10 January 1997. Journal of Atmospheric and Solar-Terrestrial Physics 61, 299–307.

Ma, S.Y., Schlegel, K., Xu, J.S., 1998. Case studies of the propagation characteristics of auroral TIDs with EISCAT CP2 data using maximum entropy cross-spectral analysis. Annales Geophysic 16, 161–167.

Maeda, S., Handa, S., 1980. Transmission of large-scale TIDs in the ionospheric F2-region. Journal of Atmospheric and Terrestrial Physics 42, 853–859.

Mannucci, A.J., Ho, C.M., Lindwister, U.J., Runge, T.F., Wilson, B.D., Yuan, D.N., 1998. A global mapping technique for GPS-drived ionospheric TEC measurements. Radio Science 33, 565.

Mercier, C., 1986. Observations of atmospheric gravity waves by radiointer-ferometry. Journal of Atmospheric and Terrestrial Physics 48, 605–624.

Natorf, L., Schlegel, K., Wernik, A.W., 1992. Gravity wave parameters derived from traveling ionospheric disturbances observations in the auroral zone. Radio Science 27 (6), 829–840.

Oliver, W.L., Otsuka, Y., Sato, M., Takami, T., Fukao, S., 1997. A climatology of F region gravity waves propagation over the middle and upper atmosphere radar. Journal of Geophysical Research 102, 14449–14512.

Rice, D.D., Hunsucker, R.D., Lanzerotti, L.J., Crowley, G., Williams, P.J.S., Craven, J.D., Frank, L., 1988. An observation of atmospheric gravity wave cause and effect during

the October 1985 WAGS campaign. Radio Science 23, 919–930.

Savina, O.N., Erukhimov, L.M., 1981. On the possible existence of a solitary internal gravity wave in a boundless isothermal atmosphere. Geomagnetizm i Aeronomiya 21 (4), 679–682.

Schaer, S., Gurtner, W., Feltens, J., 1998. IONEX: The IONosphere map eXchange format version 1. In: Dow J.W., (Ed.), Proceeding of the IGS AC Workshop, Darmstadt, Germany, February 9–11, pp. 233–247.

Sharadze, Z.S., Kvavadze, N.D., Liadze, Z.L., Mosashvili, N.V., 1986. Traveling ionospheric disturbances and the F-spread phenomenon in the mid-latitude ionosphere. Geomagnetizm i Aeronomiya 26 (1), 144–147.

Whalen, J.A., 1987. Daytime F-layer trough observed on a macroscopic scale. Journal of Geophysical Research 92, 2571–2576.

Wilson, B.D., Mannucci, A.J., Edwards, C.D., 1995. Subdaily northern hemisphere maps using the IGS GPS network. Radio Science 30, 639–648.

Yeh, K.C., Ma, S.Y., Lin, K.H., Conkright, R.O., 1994. Global ionospheric effects of the October 1989 geomagnetic storm. Journal of Geophysical Research 99 (A4), 6201–6218.